Simple Model Representations of Transport in a Complex Fracture and Their Effects on Long-Term Predictions

Chin-Fu Tsang[1], Christine Doughty[1], and Masahiro Uchida[2]

[1]Earth Sciences Division, Lawrence Berkeley National Laboratory
Berkeley, California 94720, USA

[2]Geological Isolation Research and Development Directorate, Japan Atomic Energy Agency
Akeyo-cho, Mizunami-shi, Gifu, 509-6132, Japan

Revised April 2008

Abstract

A complex fracture model for fluid flow and tracer transport was previously developed that incorporates many of the important physical effects of a realistic fracture, including advection through a heterogeneous fracture plane, partitioning of flow into multiple subfractures in the third dimension, and diffusion and sorption into fracture-filling gouge,

small altered rock matrix blocks within the fracture zone, and the unaltered semi-infinite rock matrix on both sides of the fracture zone (Tsang and Doughty, 2003). It is common, however, to represent the complex fracture by much simpler models consisting of a single fracture, with a uniform or heterogeneous transmissivity distribution over its plane and bounded on both sides by a homogeneous semi-infinite matrix. Simple-model properties are often inferred from the analysis of short-term (one to a few days) site characterization (SC) tracer-test data. The question addressed in this paper is: How reliable is the temporal upscaling of these simplified models? Are they adequate are for long-term calculations that cover thousands of years? In this study, a particle-tracking approach is used to calculate tracer-test breakthrough curves (BTCs) in a complex fracture model, incorporating all the features described above, for both a short-term SC tracer test and a 10,000-year calculation. The results are considered the “real-world”. Next, two simple fracture models, one uniform and the other heterogeneous, are introduced. Properties for these simple models are taken either from laboratory data or found by calibration to the short-term SC tracer-test BTCs obtained with the complex fracture model. Then the simple models are used to simulate tracer transport at the long-term time scale. Results show that for the short-term SC tracer test, the BTCs calculated using simple models with laboratory-measured parameters differ significantly from the BTCs obtained with the complex fracture model. By adjusting model properties, the simple models can be calibrated to reproduce the peak arrival time and height of the complex-fracture-model BTCs, but the overall match remains quite poor. Using simple models with short-term SC-calibrated parameters for long-term calculations causes order-of-magnitude errors in tracer BTCs: peak arrival time is 10–100 times too late, and peak height is 50-300 times

too small. On the other hand, using simple models with laboratory-measured properties of unfractured rock samples for 10,000-year calculations results in peak arrivals and heights up to a factor of 50 too early and large, respectively. The actual magnitudes of the errors made by using the simple models depend on the parameter values assumed for the complex fracture model, but in general, simple models are not expected to provide reliable long-term predictions. The paper concludes with some suggestions on how to improve long-term prediction calculations.

1.0 Introduction

Flow and transport in fractured rock are critical hydrological elements in many important practical problems, such as subsurface contaminant migration and safety of a nuclear waste geological repository. A review of this research area, with a discussion of trends and challenges, was presented by Neuman (2005), who also provided a comprehensive list of references. An earlier review by Tsang and Neretnieks (1998) systematically presented important field experiments on tracer transport at different spatial scales and some associated theoretical studies. During the past decade, a number of major multiyear field and modeling investigations of transport in fractured rocks have been reported. These include studies at the Mirror Lake site (Becker and Shapiro, 2003; Shapiro, 2001; Shapiro and Hsieh, 1991), the so-called TRUE project at Äspö (Andersson et al., 2004; Winberg et. al., 2003), and investigations of fractured dolomite at Carlsbad (Meigs and Beauheim, 2001; Haggerty et al., 2001; McKenna et al., 2001).

Generally, these efforts involved field measurements of migration of tracers that were introduced into a fracture or fracture system through an injection well. Data interpretation and modeling studies are used to estimate key parameters associated with transport in a fracture, such as fracture porosity or aperture and matrix diffusion coefficient. Guimerá and Carrera (2000) made an interesting study of the parameters from a large number of tracer tests and attempted to understand their dependence on spatial and temporal scales. Zhou et al (2007) also conducted a survey of measured values of the effective matrix diffusion coefficient for fractured rock at scales from meters to kilometers and showed a scale dependence with larger values for increasing spatial scale.

The parameters thus evaluated can be used in models to predict migration of tracers in fractured rocks. Using tracer migration data to determine parameters characteristic of a site is part of the site characterization (SC) process, and prediction of tracer migration tens to thousands of years into the future is part of what is known as “performance assessment” (PA). A discussion of the key issues involved in going from SC to PA is given in Tsang (2005) and also in Tsang et al. (1994). One of the issues is the development of appropriate conceptual structural models for modeling transport through fractured rock (Hodgkinson and Black, 2005; Reimus et al., 2003; Mazurek et al., 2003 and Jakob et al., 2003).

Most of the field and modeling studies to date consider a fracture to be uniform over its plane (on scales of a meter to tens or even hundreds of meters), implying that it can be characterized by its mean aperture value and a diffusion coefficient describing solute

diffusion into the surrounding rock matrix. A justification for this often-made simplification is that detailed data on deviations from this simple conceptual picture of the fracture are often not available or hard to come by. Nevertheless, there are definite field data to show that fractures are not so simple (Mazurek et al., 2001; Robinson et al., 1998; Bossart and Mazurek, 1991). The goal of the present paper is to study tracer transport in a complex fracture (defined below) and evaluate the accuracy of long-term predictions of tracer transport made by very much simplified conceptual models of the fracture. Generally, features of tracer transport that have important PA implications are the first tracer arrival time, the peak concentration, and persistence of the concentration tail. However, in this paper we do not focus on these PA issues, but rather discuss the more basic question of how well are the tracer breakthrough curves (BTC) predicted in term of their effective porosity, which controls tracer arrival time, and their effective matrix diffusion coefficient, which controls the peak concentration. These two parameters, porosity and diffusion coefficient, are also the usual ones used in analysis of tracer breakthrough curves from field tests (e.g., Chilès and deMarsily, 1993; Cvetkovic et al., 2007; Widestrand et al., 2007).

Based on geological observations presented in Mazurek et al. (2001), a complex fracture model for fluid flow and tracer transport was previously developed that incorporates many of the important physical effects of a complex fracture layer, including advection through a heterogeneous fracture plane, partitioning of flow into multiple subfractures in the third dimension, and diffusion and sorption into fracture-filling gouge, small altered rock matrix blocks within the fracture zone, and the unaltered semi-infinite

rock matrix on both sides of the fracture zone (Tsang and Doughty, 2003). Generally, the model takes its initial values for material properties from laboratory data and then modifies them by calibration to short-term SC data, such as breakthrough curves for tracer migration tests lasting one to a few days. We shall refer to these tests with duration of a few days as short-term site characterization or "stSC" data. The model can then be used for PA calculations, which track tracer migration for thousands of years, typically under much lower hydraulic gradients than are imposed during SC tracer tests. Note that SC tracer tests with duration of weeks or months are also feasible, but in the present study we assume that only short-term tests of one day's duration have been conducted.

As mentioned above, it is common to represent the complex fracture, which is considered to be the "real world" in this paper, by much simpler models consisting of a single fracture, which may have a uniform or heterogeneous transmissivity distribution over its plane and is bounded on both sides by a homogeneous semi-infinite matrix. The parameters of the simple model can be evaluated by calibration to stSC data or by laboratory measurements on core samples of rock in the vicinity of the fracture. The question posed by this paper is, how adequate are these simplified models for long-term PA calculations? It will be shown below that the stSC and PA results, corresponding to different time frames, are sensitive to different parts of the parameter set of the "real-world" complex fracture, and thus care needs to be exercised in the use of parameter values obtained from calibration with stSC tests, and perhaps much longer tests than the one-day SC test will be needed.

The paper is organized as follows. First, we present an overview of the conceptual model for the complex fracture and describe the numerical model used for the flow and transport calculations. Then, sensitivity studies of tracer breakthrough curves (BTCs) to various model parameters over a range of values are discussed. Next, two simple fracture models are introduced to represent the complex fracture model, one with a single heterogeneous fracture (without subfractures or internal materials) and the other with a uniform fracture of constant aperture. Finally, we proceed to investigate potential errors that the simple models may introduce into their long-term PA predictions. Some remarks on how to improve long-term predictions conclude the paper.

2.0 Complex Fracture Model

This section presents a brief overview of the complex fracture model developed by Tsang and Doughty (2003), where details of the model may be found. Figure 1 shows the complex fracture model, in which advection occurs in a two-dimensional (2D) heterogeneous fracture plane with a transmissivity distribution given by T(x,y), from which flow q(x,y) can be calculated given the hydraulic pressure imposed on boundaries.. Fracture structure in the third (z) dimension is accounted for by dividing flow q(x,y) among multiple subfractures. In this figure, two sub-fractures are shown, for which

$$q = q_1 + q_2 \qquad (1)$$

The partitioning of flow between subfractures is controlled by the fracture structure parameter α, by defining

$$q_2 = \alpha q_1 \qquad (2)$$

The value of α can range from 0 (only a single subfracture) to 1 (two identical subfractures). The entire fracture plane is characterized by a single α value.

Diffusion and sorption occur into three materials surrounding the fracture:

- Fault gouge within the fractures (conceptualized as small blocks of rock)
- Altered rock within the fracture zone (intermediate-size blocks of rock)
- Unaltered rock outside the fracture zone (a semi-infinite rock matrix)

The parameter controlling matrix diffusion is the effective diffusion coefficient D_e, given by $D_e = D_{fw}\phi_m\tau$, where D_{fw} is free-water diffusion coefficient, ϕ_m is matrix porosity, and τ is matrix tortuosity ($\tau \leq 1$, with $\tau = 1$ indicating a direct, nontortuous path and smaller values of τ corresponding to more tortuous paths). The sorption coefficient is K_d. Each of the three materials has its own values of K_d, ϕ_m and τ (and therefore D_e), and a characteristic length scale denoted $2r_m$.

A customized version of the numerical model THEMM (Tsang and Tsang, 2001) is used to calculate flow and transport. First, a heterogeneous 2D fracture transmissivity distribution T(x,y) is created, using program SISIM from GSLIB (Deutsch and Journel,

1998). The T field has a stochastic heterogeneity in which the correlation length can be made to depend on the T level. In our case, a larger value is used for the higher 20% of T values to represent the well-known consideration that larger transmissivity tends to be associated with a larger spatial correlation length. In general, SISIM allows anisotropic T fields, but the one created here is isotropic.

Local fracture aperture w(x,y) is assumed to be related to local T(x,y) according to the cubic law

$$T(x,y) = w^3(x,y) / [12(\mu/\rho g)] , \quad (3)$$

where μ is viscosity, ρ is fluid density, and g is acceleration due to gravity. Then, local fracture porosity $\phi_f(x,y)$ is obtained from w(x,y) according to

$$\phi_f(x,y) = 3w(x,y)/\Delta z. \quad (4)$$

where Δz is the thickness of the complex fracture zone, typically a few centimeters and assumed constant over the fracture plane, and the factor of three accounts for the fact that fractures may be oriented in any of the three spatial dimensions within the fracture zone. Mean fracture porosity ϕ_f is then defined as the porosity value obtained from Equations (3) and (4) using the geometric mean of T(x,y) in Equation (3) rather than T(x,y) itself. This derivation for $\phi_f(x,y)$ differs from the original version of THEMM, in which fracture

porosity was taken to be a constant over the entire fracture plane, equal to the mean value ϕ_f.

Table 1 summarizes the model dimensions and heterogeneous fracture properties used for the present paper, which are representative of a real fracture zone at the Äspö Underground Research Laboratory in Sweden (Doughty and Uchida, 2003).

The flow field q(x,y) is calculated by a finite-difference method, then tracer transport is calculated using particle tracking. When a particle arrives at a grid block, first an advective residence time t_w is calculated based on the 2D flow field. For the i^{th} grid block at location (x,y), denote $q(x,y) = q_i$ and $\phi_f(x,y)=\phi_{fi}$:

$$t_w = \frac{\phi_{fi}\Delta x\Delta y\Delta z}{\frac{1}{2}\sum_{j=1}^{J}|q_{ij}|} \qquad (5)$$

where q_{ij} is the flow between the i^{th} grid block and each of its *J* neighbors. Each particle is introduced into one of the two subfractures in the third dimension, which is chosen randomly, weighted by the α parameter. As the particle moves in this sub-fracture, the residence time is modified by assuming that a local cubic law holds in the subfractures (Tsang and Doughty, 2003).

Next, one of the three rock matrix materials is chosen at random, according to pre-assigned likelihoods based on the proportion of each material present, and a residence-time increment (delay) is calculated to represent diffusion and sorption into the material,

by inverting an analytical solution (Rasmuson and Neretnieks, 1981). In the analytical solution, the finite volumes of the fault gouge and altered rock within the fracture zone are accounted for, which limits their capacity for diffusion and sorption. As these finite materials become saturated, the corresponding residence-time increment decreases to zero. For a given grid block, if the residence-time increment for gouge or altered rock is less than the increment that would be obtained for the semi-infinite matrix (unaltered rock outside the fracture zone), then the semi-infinite-matrix-based increment is applied instead. This algorithm corresponds to a conceptualization in which saturated gouge and altered rock do not shield the fluid particles from interacting with the semi-infinite matrix. In previous studies (Tsang and Doughty, 2003), we used a different conceptualization, in which fluid particles encountering saturated gouge or altered rock did not have a chance to interact with the semi-infinite matrix. It turns out that for SC time scales, tracer BTCs produced by the two prescriptions only differ in their late-time tails, with identical peak arrival times and heights. In contrast, for PA time scales, the two prescriptions produce BTCs that differ from each other. The present prescription has the advantage that when the gouge and intermediate blocks are saturated, the BTCs tend to the simple case of diffusion into the bounding semi-infinite rock matrix.

For the present studies we consider two different tracers, tritiated water (HTO), which is nonsorbing, and Sr, which is slightly sorbing. Table 2 summarizes the properties of the three rock matrix materials, which were obtained from laboratory measurements and by calibrating the complex fracture model to a tracer test conducted using two boreholes packed off in the fracture zone at Äspö, Sweden (Doughty and Uchida, 2003). Note that

the parameters for effective diffusion and sorption are much higher for gouge material and intermediate blocks than the semi-infinite rock matrix because they have undergone much larger mechanical and chemical disturbances than the intact rock corresponding to the semi-infinite matrix.

Tracer transport is calculated for a pulse tracer release in a steady-state flow field. For SC, the flow field represents a radially converging tracer test with tracer traveling about 5 m and breakthrough observed over a few days Pumping rate, test duration, and well separation are based on the parameters of an actual tracer experiment conducted at Äspö Hard Rock Laboratory (Doughty and Uchida, 2003). For PA, a natural hydraulic gradient creates a linear flow field. Tracer is released over a 2 m wide zone and collected over a 15 m wide zone, 10 m downgradient from the release location. Tracer arrivals occur over thousands of years. Table 3 summarizes the characteristics of the two flow fields. Note that hydraulic gradient is several orders of magnitude larger for the SC flow field than for the PA flow field, to enable the SC tracer test to be conducted within a reasonable time frame. Figure 2 illustrates the heterogeneous T field and the PA flow field. The T field is moderately heterogeneous, causing localized channels of preferential flow to develop (Moreno and Tsang, 1994; Tsang and Tsang, 1989).

3.0 Sensitivity of Tracer Breakthrough Curves to Features of Complex Fracture Model

The key output of the complex fracture model is the tracer breakthrough curve (BTC), that is, the tracer concentration C as a function of time at a specified location, which is represented by a single well for SC and the downgradient boundary of the fracture model for PA. For a pulse tracer release, the key characteristics of the tracer BTC (Chilès and deMarsily, 1993) may be defined as:

- Peak arrival time t_{pk}
- Peak height C_{pk}
- Peak shape - quantified by the first arrival time t_1 (which we take as the time at which $C \approx 10^{-3}C_{pk}$) and the rate of decrease in the tail region

Figure 3 illustrates stSC tracer BTCs for the complex model with parameters given in Tables 1-2, with the three points t_{pk}, C_{pk}, and t_1 marked. In the subsections below, we examine the impact of various features of the complex fracture model on these BTC characteristics.

3.1 Fracture Heterogeneity

To explore the effect of heterogeneity over the fracture plane on tracer BTCs, we conducted a series of short-term site characterization (stSC) simulations omitting matrix diffusion and sorption. Thus, tracer transport occurs purely by advection through the fracture. Moreover, we consider only one subfracture by taking $\alpha = 0$. The top frame of Figure 4 shows the resulting tracer BTCs for T fields with four levels of heterogeneity (created by increasing σ_{logT} in the heterogeneous field generator, SISIM, while keeping all other parameters unchanged). As σ_{logT} increases, the peak height decreases, the peak becomes broader, and the peak arrival time is delayed. The lowering of peak height and

broadening of peak width occur as more diverse flow paths are encountered within the more variable T fields. The peak arrival is delayed because fluid flows preferentially into localized high transmissivity regions, which have high fracture porosity and consequently a longer advective residence time. The bottom frame of Figure 4 shows the corresponding tracer BTCs obtained with the full complex fracture model, with two subfractures and three materials for matrix diffusion and sorption. All peaks are later, lower, and broader due to the addition of matrix diffusion, and they show a small second peak arising from flow through the smaller of the two subfractures. However, the effect of increasing fracture heterogeneity is unchanged.

Work elsewhere (Moreno and Tsang, 1994) has shown that for even larger values of $\sigma_{\log T}$ (e.g., 3), earlier and sharper peaks may develop as flow becomes so focused that large portions of the fracture network are bypassed. This is the strong channeling case. In such a case, the early peak is accompanied by a long late-time tail which includes effects of diffusion not only into rock matrix, but also into "stagnant" water region between channels in the fracture plane. The value of $\sigma_{\log T} = 1.35$ (Table 1) used in the current study has not reached this regime.

3.2 Mean Fracture Porosity ϕ_f

The mean fracture porosity ϕ_f controls the peak arrival time, with arrival time longer as ϕ_f increases. The peak height also decreases with increasing ϕ_f, as the slower travel time allows more matrix diffusion and sorption to occur. Figure 5 shows stSC tracer BTCs for five values of ϕ_f. Note that ϕ_f is the fraction of void space within the complex fracture zone, not within the fractured rock block as a whole. In this sensitivity

calculation, we have varied ϕ_f without changing T, which is not internally consistent, but this is often done in calibration exercises, in which measured T values are used in tracer transport modeling and ϕ_f is independently varied to match the BTCs (see, e.g., Chilès and deMarsily, 1993; Cvetkovic et al., 2007; Widestrand et al., 2007)

3.3 Fracture Structure Parameter α

Fracture structure parameter α, corresponding to the ratio of flows through the two subfractures, can range from 0 to 1. Figure 6 shows stSC tracer BTCs for ten α values within this range. For $\alpha = 0$, there is only one subfracture, and for $\alpha = 1$, there are two identical subfractures, so in both of these two cases the shape of the BTCs is controlled by fracture heterogeneity (compare Figure 4). For the smallest non-zero α value (0.01), the fraction of flow occurring through the smaller subfracture, $q_2 = \alpha q_1$, is so small that it does not affect the BTC noticeably. For $\alpha = 0.03$, the peak arrival time and height are unchanged, but a second, much smaller and much later peak is present, reflecting flow through the smaller subfracture. For $\alpha \geq 0.1$, flow through the smaller subfracture is significant enough to delay the arrival and decrease the height of the main peak (less flow through the larger subfracture). For $\alpha \geq 0.5$, no individual second peak is visible, but an extended tail of the main peak shows the contribution of flow through the smaller subfracture. For $\alpha = 1$, the two identical subfractures provide greater fracture porosity than a single subfracture ($\alpha = 0$) does. This ϕ_f dependence on α can be explained by considering that the two subfractures each obey the cubic law (Equation 3), and that the sum of their flows or transmissivities is fixed (Equation 1). This means that $(w_1^3 + w_2^3) =$

342 $w_1^3(1+\alpha)$ = constant, so that porosity (Equation 4), being proportional to $(w_1 + w_2)$ =
343 $w_1(1+\alpha^{1/3})$, becomes a function of α. From this it can be shown directly that the α=1 case
344 has a larger porosity and thus would have a later, lower peak. Note that for small α
345 values, if monitoring does not continue long enough or measurement sensitivity is not
346 high enough, the second peak may not be observed. Then the only observable effect of
347 increasing α will be to delay arrival time and decrease the height of the peak, much like
348 the effect of increasing ϕ_f.
349

350 ***3.4 Matrix Diffusion and Sorption***

351 The time-scale on which matrix diffusion and sorption occur depends strongly on the
352 diffusion properties of the rock blocks, with the gouge having the fastest diffusion and
353 strongest sorption (until it is saturated), and the semi-infinite matrix having the slowest
354 diffusion and weakest sorption. Figure 7 shows tracer BTCs for stSC tracer tests with a
355 nonsorbing tracer for the full complex fracture model, with diffusion into three matrix
356 materials, and for two variations: one with diffusion occurring only into the gouge
357 material and the other with diffusion occurring into the gouge and intermediate-size
358 matrix blocks within the fracture zone, but not into the semi-infinite matrix outside the
359 fracture zone. For all cases, α=0.03.
360

361 It is apparent that for tracer tests lasting a few days, the calculated BTC is essentially
362 insensitive to diffusion into the semi-infinite rock matrix; it is nearly two days before the
363 full complex fracture model BTC differs appreciably from the BTCs for the cases with no
364 diffusion into semi-infinite rock. Moreover, for the period including the tracer peak, the

BTC is primarily controlled by diffusion into the gouge. Hence, a stSC tracer test provides the most information on gouge properties, some limited information on intermediate-size matrix blocks, and little if any information on the semi-infinite rock matrix properties. Longer tests would be required for the intermediate-size matrix blocks and the semi-infinite matrix to have a noticeable effect on stSC tracer BTC.

4.0 Simple Fracture Models and an Approach to Study the Relationship between SC-calibrated, Laboratory-measured and PA Transport Parameters

The previous two sections present the complex fracture model and how the breakthrough curves (BTCs) of tracer transport through it depend on its parameters. In practical field studies of flow and transport through fractures, such detailed parameters of a complex fracture are normally not available. Often a single fracture (i.e., no subfractures) with a constant aperture (constant transmissivity) over its plane is used to represent the complex fracture. The focus of this and following sections is to study whether such a simplified representation of the complex fracture (which is taken as the "real world") can adequately reproduce flow and transport, and what errors are introduced into long-term prediction of tracer BTCs by such a simplification.

Instead of one simple fracture model, we shall consider two models, both of which account for advection through a planar fracture and diffusion and sorption into a homogeneous semi-infinite rock matrix. In one case, the fracture has a uniform transmissivity T over its plane, and in the other case, it has the same heterogeneous

T(x,y) field as in the complex fracture model. Here it is assumed that the T(x,y) for the heterogeneous model is known. Then the geometric mean transmissivity <T> is used as the transmissivity for the simple uniform model. Once <T> and T(x.y) are defined, the only parameters in either of the two simple models are ϕ_f and D_e. The features present in the complex fracture model that are absent from both the simple models are the partitioning of flow between multiple subfractures, and diffusion and sorption into gouge and finite blocks of altered rock within the fracture zone. These will be accounted for approximately through the use of "effective values" of ϕ_f and D_e.

We use the complex fracture model to produce tracer BTCs for both stSC and PA time scales and conditions, which are the synthetic "real world" results. We then apply the two simple fracture models to stSC and PA problems and compare the resulting tracer BTCs to those of the complex fracture model, adjusting the simple model parameter values of ϕ_f and D_e to optimize the match. There are three sets of effective values of ϕ_f and D_e that will be used in the discussions below:

- $\phi_{f\,(SC)}$ and $D_{e\,(SC)}$, values resulting from calibration against stSC data, which are from tracer tests of short durations of a few days.
- $\phi_{f\,(PA)}$ and $D_{e\,(PA)}$, values resulting from fitting against PA results of the complex model (the 'real world"). This is of course not something that can be obtained in field cases. Here they are calculated and used for comparison with other effective values to study errors made in extrapolation to long-term predictions.
- $\phi_{f\,(Lab)}$ and $D_{e\,(Lab)}$, values obtained by laboratory measurements on rock samples from the two sides of the complex fracture. These laboratory-determined

parameter values correspond to the semi-infinite rock matrix values used in the complex fracture model.

5.0 Results

5.1 SC Calibration

Figure 8 shows the tracer BTCs for nonsorbing HTO and slightly-sorbing Sr, under stSC conditions (a converging radial tracer test) for the complex fracture model, considering two different values of fracture structure parameter α, with the upper frame of the figure showing the case of α=0 and the lower frame showing α=0.6. Also presented in the figure are the BTCs obtained from a simple heterogeneous fracture model using (a) the $D_{e\,(Lab)}$ and $\phi_{f\,(Lab)}$ values and (b) the calibrated $D_{e\,(SC)}$ and $\phi_{f\,(SC)}$ values. For reference, a tracer BTC for an advection-only model (heterogeneous fracture, α = 0, no rock matrix) is also plotted. Because the different diffusion and sorption coefficients of HTO and Sr only affect interactions with the rock matrix, the advection-only models for HTO and Sr yield identical BTCs. The simple models with laboratory parameters also yield nearly indistinguishable BTCs for HTO and Sr. This is expected, considering that the parameter groups controlling matrix diffusion, $D_e\phi_m$ for non-sorbing HTO and $D_eK_d\rho_p$ for slightly-sorbing Sr, happen to be nearly the same (see Table 2).

The complex fracture model BTC is significantly different from the advection-only BTC, with a later, lower, broader peak. In contrast, the heterogeneous simple fracture model BTCs for the original values of D_e and ϕ_f (i.e., $D_{e\,(Lab)}$ and $\phi_{f\,(Lab)}$) differ from the

advection-only BTC only at late times, showing a longer tail. This implies that in our case for the SC time scale, the features present only in the complex fracture model—flow through multiple subfractures and diffusion and sorption into gouge and intermediate-size matrix blocks—have a significant impact, whereas diffusion and sorption into the semi-infinite matrix have a minor effect. By increasing D_e and ϕ_f (see Table 4), the simple model can match the timing, height, and width of the peak of the complex model BTCs, although the details of the tails of the BTCs are not well matched. Increasing α from 0 to 0.6 results in somewhat lower and later peaks, requiring larger values of $D_{e\,(SC)}$ and $\phi_{f\,(SC)}$. Note that in this discussion, a comparison is made between the complex fracture model and the calibrated simple models. In practice, increased D_e and ϕ_f can be due to other physical effects such as micro-fractures on both sides of the fracture plane.

Figure 9 shows the analogous results to Figure 8 for the uniform simple fracture model. The advection-only BTC for a uniform fracture is much narrower than that for the heterogeneous fracture. The uncalibrated simple model BTCs (obtained with $D_{e\,(Lab)}$ and $\phi_{f\,(Lab)}$) differ from the advection-only BTC only at late times, confirming that diffusion and sorption into the semi-infinite matrix are too slow to affect peak timing or height. By increasing D_e and ϕ_f (see Table 4), the calibrated simple model BTCs can match the peak arrival time and height of the complex model BTCs, but the peaks remain too narrow, a consequence of the lack of heterogeneity in the fracture plane.

Table 4 summarizes the parameter values required to match the stSC tracer BTCs shown in Figure 8 and Figure 9. D_e must be increased by a factor of 100–700 for the

heterogeneous simple model and by a factor of 3,000–12,000 for the uniform simple model, and ϕ_f must be increased by a factor of 4–12 for the heterogeneous simple model and by a factor of 13–34 for the uniform simple model. These increases delay, broaden, and lower the height of the peak, thus mimicking the features of the complex model that are missing from the simple models: principally the enhanced diffusion and sorption that occur in the fault gouge and altered rock matrix within the complex fracture zone. The larger increases required for the uniform simple model reflect the additional broadening process, fracture heterogeneity, which is missing from the uniform simple model.

The left-hand column of Figure 10 summarizes the results of the SC calibration of the heterogeneous and uniform simple models for a range of α values. Increasing α results in greater pore space for fluid flow, thus requiring increases in $\phi_{f\,(SC)}$. Intermediate values of α provide the best opportunity for flow along disparate pathways, with the most significant spreading of tracer arrival times, and these cases therefore require the largest values of $D_{e\,(SC)}$.

5.2 PA Calibration

Figure 11 shows the tracer BTCs for nonsorbing HTO and slightly-sorbing Sr, under PA conditions (long-term and linear flow under a regional head gradient) for the complex fracture model, considering two values of α, and the BTCs for a heterogeneous simple fracture model. For the simple model, BTCs obtained using the original values $D_{e\,(Lab)}$ and $\phi_{f\,(Lab)}$, and calibrated values $D_{e\,(SC)}$, $\phi_{f\,(SC)}$, $D_{e\,(PA)}$, and $\phi_{f\,(PA)}$ are all shown. Also plotted is a tracer BTC for an advection-only model (heterogeneous fracture, $\alpha = 0$, no

rock matrix), for which HTO and Sr yield identical BTCs. The complex fracture model shows a later, lower, broader peak than does the advection-only model, along with a much longer tail, indicating that matrix diffusion and sorption are important processes at PA time scales. With the laboratory parameters, the simple model produces a peak arrival time that is 3–10 times too early and a peak height that is 2–10 times too high, indicating that fracture porosity, matrix diffusion, and sorption are being underestimated. When using the stSC-calibrated parameters, the simple model produces a peak arrival time that is 10–20 times too late and a peak height that is 50–100 times too small, indicating that fracture porosity, matrix diffusion, and sorption are being greatly overestimated. By calibration to the PA tracer curves, a good match to the peak arrival time, height, width, and tail can be obtained for the heterogeneous simple fracture model.

Figure 12 shows the analogous results to Figure 11 for the uniform simple fracture model. The general features of the original, stSC-calibrated, and PA-calibrated simple models are similar to those shown in Figure 11 for a heterogeneous simple model: with the laboratory parameters, peak arrival time is 10–30 times too early and peak height is 10–50 times too high. With the stSC-calibrated parameters, peak arrival time is about 100 times too late and peak height is 100–300 times too small. Moreover, the shape of the BTC for the PA-calibrated uniform simple model does not match the complex model result as well as did the heterogeneous simple model, producing too narrow a peak, indicating that the effect of fracture heterogeneity cannot be correctly reproduced merely by using effective values of fracture porosity, matrix diffusion, and sorption.

503 Table 4 summarizes the parameter values required to match the PA tracer BTCs
504 shown in Figure 11 and Figure 12. D_e must be increased by a factor of 2–9 for the
505 heterogeneous simple model and by a factor of 12–48 for the uniform simple model; ϕ_f
506 must be increased by a factor of 5–13 for the heterogeneous simple model and by a factor
507 of 9–20 for the uniform simple model. The center column of Figure 10 summarizes the
508 results of the PA calibration of the heterogeneous and uniform simple models for a range
509 of α values. The α dependence is very similar to that for stSC, with $\phi_{f\,(SC)}/\phi_{f\,(Lab)}$ steadily
510 increasing with increasing α, and D_e (SC)/D_e (Lab) showing a modest maximum for
511 intermediate values of α.
512
513 As described above, the serious errors made when using a simple model with SC-
514 calibrated parameters for a PA simulation (Figures 11 and 12) arise because stSC time-
515 scale processes are dominated by fracture gouge properties, whereas PA-time-scale
516 processes are dominated by semi-infinite matrix properties. The results shown in Figures
517 11 and 12 employ a population fraction that is 25% gouge and 25% intermediate-size
518 matrix blocks. It is worthwhile to see if errors become negligible when the fractions of
519 fracture gouge and intermediate-size matrix blocks are much smaller. Complex fracture
520 models with $\alpha = 0$ and $\alpha = 0.6$, each with population fractions 10% gouge and 10%
521 intermediate-size matrix blocks, were used to simulate stSC and PA time-scale tracer
522 tests. Uniform and heterogeneous simple models were calibrated to the stSC tracer tests,
523 and the resulting values of $\phi_{f\,(SC)}$ and $D_{e\,(SC)}$ were used to simulate the PA time-scale
524 tracer test. Results (not shown) indicate that the errors made when simulating PA with
525 SC-calibrated properties for the are 10% gouge, 10% intermediate case are comparable to

errors obtained for the 25% gouge, 25% intermediate case. Considering that the diffusion and sorption properties of the fault gouge and unaltered rock differ by up to three orders of magnitude (Table 2), it is perhaps not surprising that merely decreasing the percent of gouge from 25% to 10% has only a minor effect. The lesson is that even fracture systems with small percentages of gouge and altered rock can exhibit very different behavior than do simple systems with only unaltered rock matrix surrounding the fractures.

5.3 Comparison of PA-calibrated transport parameters, SC-calibrated, and Laboratory-measured parameters

In Table 4, calibrated parameters are compared with laboratory-measured parameters. The table entries show the parameter changes required to mimic the processes of the complex fracture model that are missing in the simple models. In the complex model, both the non-zero α and large gouge diffusion delay peak arrival; this is accomplished in the simple models by modest increases in ϕ_f, which lengthen advective residence time. In the complex model, the presence of gouge material enhances matrix diffusion, delaying, lowering, and broadening the tracer peak; this is mimicked in the simple models with large increases in D_e. Fracture heterogeneity has a similar effect on the tracer peak, so even larger increases in D_e are required for the uniform simple model.

In Table 5 and the right-hand column of Figure 10, SC-calibrated parameters are compared with PA-calibrated parameters. Note that if the flow and transport processes did not have a strong time dependence—that is, if SC and PA processes were essentially the same—then all the entries in Table 5 would be one. The $\phi_{f\,(SC)}/\phi_{f\,(PA)}$ ratios do not, in

fact, differ significantly from one, which is consistent with the notion that ϕ_f primarily controls advective residence time, a quantity that does not have a strong time dependence. In contrast, the $D_{e\,(SC)}/D_{e\,(PA)}$ ratios are much greater than one, because matrix diffusion is dominated by gouge diffusion at SC time scales and by semi-infinite matrix diffusion at PA time scales.

6.0 Discussions and Conclusions

We have examined the possibility of using simple fracture models, consisting of a planar fracture, which may have a uniform transmissivity or a heterogeneous transmissivity distribution, and which is bounded on either side by a homogeneous semi-infinite rock matrix, to represent a complex fracture model (the "real world"). The latter includes a heterogeneous transmissivity distribution, as well as multiple subfractures, and diffusion and sorption into fracture-filling gouge and intermediate-size, altered rock matrix blocks, and the semi-infinite rock matrix on either side of the fracture. The study is based on comparing the effective parameters required for the simple models to reproduce PA results at 10,000 years and SC results from stSC tracer tests as calculated by the complex model (considered "the real world"). We find that by adjusting fracture porosity ϕ_f and semi-infinite matrix diffusion coefficient D_e, simple fracture models can reproduce the key features of an SC tracer test: peak height and timing are well matched, while the BTC tail misses some detail. For a simple model with a uniform fracture transmissivity distribution, the leading edge of the BTC is too sharp. PA tracer arrivals can be matched comparably well, but the required effective D_e values differ by up to two

orders of magnitude from those obtained by stSC calibration with tracer duration of a few days. Using stSC-calibrated parameters for PA calculations with the simple models causes order-of-magnitude errors in tracer BTCs: peak arrival time is 10–100 times too late and peak height is 50–300 times too small.

On the other hand, using laboratory-measured parameters of rock samples from unfractured rock for PA calculations also produces erroneous results: peak arrivals and heights can be up to a factor of 50 too early and high, respectively. These conclusions are strongly dependent on the material properties of the fracture gouge, intermediate blocks, and the semi-infinite medium used in the complex model. For example, they can be opposite to what are stated if the matrix diffusion-sorption properties of the intermediate blocks are weaker than those of the semi-infinite rocks on either side of the complex fracture.

Thus, we conclude that simple models do not provide a reliable means of making PA predictions, if stSC data are all that are available for calibration. Significant, though smaller, errors are also introduced if laboratory-measured values are used. We suggest that using a more realistic complex fracture model to interpret SC tracer test data could enhance confidence of PA prediction and also allow temporal upscaling, especially when tracer tests of a longer term than a few days are conducted. Further studies are under way to evaluate the additional information that could be extracted from tracer tests of longer durations. Preliminary calculations considering tracer tests of weeks to months' duration show that, for our set of parameters, the gouge material and intermediate blocks gradually

become saturated with tracers for longer tests, so that the BTCs display more and more the effects of the semi-infinite matrix. We are optimistic that by a combination of short and long-term tracer tests we may be able to evaluate the appropriate parameter values for long-term prediction of tracer transport. It should also be noted that using the complex model directly as a basis for SC data analysis (even with a shortage of data and non-uniqueness of parameters) has certain advantages, because it allows us to evaluate effects of gouge materials in the fracture that are often observed in the field and to provide a way to estimate uncertainties involved in long-term tracer transport calculations.

The present paper represents a first step in studying relationships between parameters from laboratory experiments or from short-term tracer transport experiments and long-term prediction of tracer transport for thousands of years, for the particular case of a complex fracture. The actual real world involves features not in our complex fracture model, such as micro-fractures on both sides of the fracture plane and flow across multiple fractures in a network. Our study indicates the danger of presumptuously modeling fractures or fault zones as simple fractures with homogeneous properties. There is a need to have some information, even at a rough level, on the complexity of fractures and fracture zones. Then such information can be used to improve prediction calculations and also, by sensitivity analysis, to estimate the uncertainty ranges of the predictions, which are a very important part of any long-term predictions.

Acknowledgments

We thank Kenzi Karasaki of Berkeley Lab and the anonymous WRR reviewers for their careful review of this paper and most helpful comments. This work was supported by the Japan Atomic Energy Agency (JAEA) under the Binational Research Cooperative Program between JAEA and the Director, Office of Civilian Radioactive Waste Management, of the U.S. Department of Energy under Contract No. DE-AC02-05CH11231.

References

Andersson, P, J. Byegård, E.-L. Tullborg, T. Doe, J. Hermanson, and A. Winberg, In situ tracer tests to determine retention properties of a block scale fracture network in granitic rock at the Äspö Hard Rock Laboratory, Sweden. *J Cont Hydrology*, 70, pp 271-297, 2004.

Becker, M.W., and A.M. Shapiro, Interpreting tracer breakthrouh tailing from different forced-gradient tracer experiment configurations in fractured bedrock. *Water Resour Res*, 39(1), 1024, DOI: 10.1029/2001WR00190, 2003.

Bossart, P. and M. Mazurek, Grimsel Test Site-structural geology and water flow-paths in the migration shear-zone. *NAGRA Tech Rep NTB 91-12*, Nagra, Wettingten, Switzerland, 1991.

640 Brown, S.R., A. Caprihan, and R. Hardy, Experimental observation of fluid flow
641 channels in a single fracture *J Geophys Res*, 103(B3), 5125–5132, 1998.
642
643 Chilès, J.-P. and G. deMarsily, Stochastic models of fracture systems and their use in
644 flow and transport modeling. Book Chapter in *Flow and Contaminant Transport in*
645 *Fractured Rocks,* edited by J. Bear, G. deMarsily and C. F. Tsang, Academic Press, pp.
646 169-236, 1993.
647
648 Cvetkovic, V., H. Cheng, H. Widestrand, J. Byegård, A. Winberg, and P. Andersson,
649 Sorbing tracer experiments in a crystalline rock fracture at Äspö (Sweden): 2. Transport
650 modeling and effective parameter estimation, *Water Resour Res*, 43, W11421,
651 doi:10.1029/2006WR005278, 2007.
652
653 Doughty, C. and M. Uchida, PA calculations for feature A with third-dimension structure
654 based on tracer test calibration, *Rep. IPR-04-33,* Swedish Nuclear Fuel and Waste
655 Management Co. (SKB), Stockholm, 2003.
656
657 Deutsch, C.V. and A.G. Journel, GSLIB: *Geostatistical software library and user's*
658 *guide*, 2nd ed., Oxford Univ. Press, New York 1998.Mazurek et al., 2001.
659
660 Guimerá, J., and J. Carrera, A comparison of hydraulic and transport parameters
661 measured in low-permeability fractured media, *J Cont Hydrology,* 41, 261–281, 2000.
662

663 Haggerty, R.R., S.W. Fleming, L.C. Meigs, and S.A. McKenna, Tracer tests in a
664 fractured dolomite, 2. Analysis of mass transfer in single-well injection-withdrawal tests.
665 *Water Resour Res* 37(5) 1129–1142, 2001.
666
667 Hodgkinson, D., and J. Black, Äspö Task Force on modelling of groundwater flow and
668 transport of solutes: Review of Tasks 6A, 6B, and 6B2, *SKB Tech Rep TR-05-14*, Svensk
669 Karnbranslehantering AB (SKB) Swedish Nuclear Fuel and Waste Management Co,
670 2005.
671
672 Jakob, A, M. Mazurek, and W. Heer, Solute transport in crystalline rocks at Äspö II:
673 Blind predictions, inverse modelling and lessons learnt from test STTI. *J Cont*
674 *Hydrology*, 61, 175-190, 2003.
675
676 Mazurek, M., P. Bossart, and J. Hermanson, Classification and characterization of water-
677 conducting features at Äspö, in *Proceedings of International Seminar First TRUE Stage*
678 *Rep. TR-01-24*, pp. 203-208, Swedish Nuclear Fuel and Waste Management Co. (SKB),
679 Stockholm, 2001.
680
681 Mazurek, M, A. Jakob, and P. Bossart, Solute transport in crystalline rocks at Äspö -I:
682 Geological basis and model calibration. *J Cont Hydrology*, 61, 157-174, 2003.
683

McKenna, S.A., L.C. Meigs, and R.R. Haggerty, Tracer tests in a fractured dolomite, 3. Double porosity, multiple-rate mass transfer processes in convergent flow tracer tests. *Water Resour Res*, 37(5) 1143–1154, 2001.

Meigs, L.C., and R.L. Beauheim, Tracer tests in fractured dolomite, 1. Experimental design and observed tracer recoveries, *Water Resour Res*, 37(5) 1113–1128, 2001.

Moreno, L., and C. F. Tsang, Flow channeling in strongly heterogeneous porous media: A numerical study, *Water Resour Res*, 30 (5), 1421–1430, 1994.

Neuman, S.P., Trends, prospects, and challenges in quantifying flow and transport through fractured rocks, *Hydrogeol Jour*, 13, 124–147, 2005.

Rasmuson, A. and I. Neretnieks, Migration of radionuclides in fissured rock: The influence of micropore diffusion and longitudinal dispersion, *J. Geophys Res*, 86(B5), 3749–3758, 1981.

Reimus, P, G. Pohll, T. Mihevc, J. Chapman, M. Raga, B. Lyles, S. Kosinski, R. Niswonger, and P. Sanders, Testing and parameterizing a conceptual model for solute transport in a fractured granite using multiple tracers in a forced gradient test. *Water Resour Res* 39(12), 1356, DOl: 10.1029/ 2002WRR001597, 2003.

706 Robinson, N., J.M. Sharp, Jr., and I. Kreisel, Contaminant transport in sets of parallel
707 finite fractures with fracture skins. *J Cont Hydro1ogy,* 3l, 83–109, 1998.
708
709 Shapiro, A.M., Effective matrix diffusion in kilometer-scale transport in fractured
710 crystalline rock. *Water Resour Res*, 37(3), 507–522, 2001.
711
712 Tsang, C.-F. Is Current Hydrogeologic Research Addressing Long-Term Predictions?
713 *Ground Water*, 43 (3), 296–300. 2005.
714
715 Tsang, C.-F. and C. Doughty, A particle-tracking approach to simulating transport in a
716 complex fracture, *Water Resour Res,* 39(7), 1174, doi:10.1029/2002WR001614, 2003.
717
718 Tsang, C.-F., L. Gelhar, G. de Marsily, and J. Andersson, Solute transport in
719 heterogeneous media: A discussion of technical issues coupling site characterization and
720 predictive assessment. *Adv in Water Resour*, 17 (4), 259–264, 1994.
721
722 Tsang, C.-F. and I. Neretnieks, Flow channeling in heterogeneous fractured rocks. *Rev*
723 *Geophys*, 36(2), 275–298, 1998.
724
725 Tsang, Y.W. and C.-F. Tsang, Flow channeling in a single fracture as a two-dimensional
726 strongly heterogeneous permeable medium, *Water Resour Res*, 25 (9), 2076–2080, 1989.
727

728 Tsang, Y.W. and C.-F. Tsang, A particle-tracking method for advective transport in
729 fractures with diffusion into finite matrix blocks, *Water Resour Res*, 37(3), 831–835,
730 2001.
731
732 Widestrand, H., J. Byegård, V. Cvetkovic, E.-L. Tullborg, A. Winberg, P. Andersson, and
733 M. Siitari-Kauppi, Sorbing tracer experiments in a crystalline rock fracture at Äspö
734 (Sweden): 1. Experimental results and micro-scale characterization of retention
735 properties, *Water Resour Res*, 43, W10413, doi:10.1029/2006WR005277, 2007.
736
737 Winberg, A, P. Andersson, A. Poteri, V. Cvetkovic, W. Dershowitz, J. Hermanson, J.J.
738 Gomez-Hernandez, A. Hautojarvi, D. Billaux, E.-L. Tullborg, D. Holton, P. Meier, and
739 A. Medina, Final report of the TRUE Block Scale project, 4. Synthesis of flow, transport
740 and retention in the block scale. *SKB Technical Report TR-02-16,* Swedish Nuclear Fuel
741 and Waste Management Co., Stockholm, Sweden, 2003.
742
743 Zhou, Q., H.H. Liu, F.J. Molz, Y. Zhang, and G.S. Bodvarsson, Field scale effective
744 matrix diffusion coefficient for fractured rock: Results from literature survey. *J Cont*
745 *Hydrology*, 93, 161-187, 2007.

746 **Tables**

747

748 Table 1. Model dimensions and heterogeneous fracture properties for a reference case

749 that is representative of a real fracture (Doughty and Uchida, 2003).

Parameter	Value
Fracture dimensions (m)	15, 15, 0.02
nx, ny, nz (number of grid blocks)	150, 150, 1
Δx, Δy, Δz (m) (grid spacing)	0.10, 0.10, 0.02
Sequential indicator simulation using a CDF for $\log_{10}T$ based on 15 well-test analyses for 5 boreholes	
Mean, standard deviation $\log_{10}T$ (T in m^2/s)	-6.5, 1.35
Spherical variogram range – for lower 80% of T values	0.3 m
Spherical variogram range – for higher 20 % of T values	1 m
Mean fracture porosity ϕ_f	0.011
Fracture structure parameter α	0.03

750 Table 2. Properties of three rock matrix materials for a reference case that is

751 representative of a real fracture (Doughty and Uchida, 2003).

	Small blocks (fault gouge)	Intermediate blocks (altered rock inside ladder structure)	Semi-infinite matrix (unaltered rock outside ladder structure)
Proportion	0.25	0.25	0.5
Radius r_m (m)	$5 \cdot 10^{-4}$	0.005	not applicable (essentially infinite)
Porosity ϕ_m	0.2	0.01	0.004
Tortuosity τ	0.625	0.0625	0.0125
Density ρ_p (kg/m^3)	2700	2700	2700
D_{fw} (m^2/s)	HTO: $2.35 \cdot 10^{-9}$ Sr: $7.90 \cdot 10^{-10}$		
Effective Diffusion Coefficient D_e (m^2/s)	HTO: $2.9 \cdot 10^{-10}$ Sr: $9.9 \cdot 10^{-11}$	HTO: $1.5 \cdot 10^{-12}$ Sr: $4.9 \cdot 10^{-13}$	HTO: $1.2 \cdot 10^{-13}$ Sr: $4.0 \cdot 10^{-14}$
Sorption coefficient K_d (m^3/kg)	HTO: 0 Sr: $1.5 \cdot 10^{-4}$	HTO: 0 Sr: $4.7 \cdot 10^{-6}$	HTO: 0 Sr: $4.7 \cdot 10^{-6}$

752 Table 3. Comparison of flow fields for SC and PA.

	Site Characterization (SC): Two-well tracer test	Performance Assessment (PA): Natural gradient
Flow field	Radial converging (Q = 0.4 L/min, hydraulic gradient approximately 1 m/m)	Linear (hydraulic gradient 0.001 m/m)
Tracer injection period	10 minutes	1 day
Particle release location	One well	2 m wide zone
Particle collection location	One well, 5 m away from release location	15 m wide zone (width of fracture), 10 m down-gradient from release location
Time of tracer observation	Main peak; 1-2 days Tail: up to 2 months	Peak: 1-5 years Tail: up to 2,000 years

753 Table 4. Summary of parameter values required in Figures 8–12 for simple models to

754 match SC and PA tracer BTCs produced by the complex fracture model.

		SC		PA	
		Heterogeneous	Uniform	Heterogeneous	Uniform
$\alpha = 0$		$\phi_{f\,(SC)}/\phi_{f\,(Lab)}$		$\phi_{f\,(PA)}/\phi_{f\,(Lab)}$	
	HTO	4.5	13	5.3	9.0
	Sr	8.0	23	9.5	17
		$D_{e\,(SC)}/D_{e\,(Lab)}$		$D_{e\,(PA)}/D_{e\,(Lab)}$	
	HTO	120	2,800	1.8	12
	Sr	236	4,724	2.0	13
$\alpha = 0.6$		$\phi_{f\,(SC)}/\phi_{f\,(Lab)}$		$\phi_{f\,(PA)}/\phi_{f\,(Lab)}$	
	HTO	7.0	19	7.4	9.5
	Sr	12	34	13	20
		$D_{e\,(SC)}/D_{e\,(Lab)}$		$D_{e\,(PA)}/D_{e\,(Lab)}$	
	HTO	400	6,800	7.6	42
	Sr	709	11,811	8.8	48

755 Table 5. Comparison of SC-calibrated parameters with PA-calibrated parameters. The
756 ratios shown are for $\alpha = 0$, but the right-hand column of Figure 10 shows that the ratios
757 are not very sensitive to α.

Two simple models		Heterogeneous	Uniform
Fracture porosity factor $\phi_{f\,(SC)}/\ \phi_{f\,(PA)}$	HTO	0.85	1.44
	Sr	0.84	1.35
Diffusion factor (semi-infinite rock) $D_{e\,(SC)}\ /D_{e\,(PA)}$	HTO	65	233
	Sr	118	369

Figures

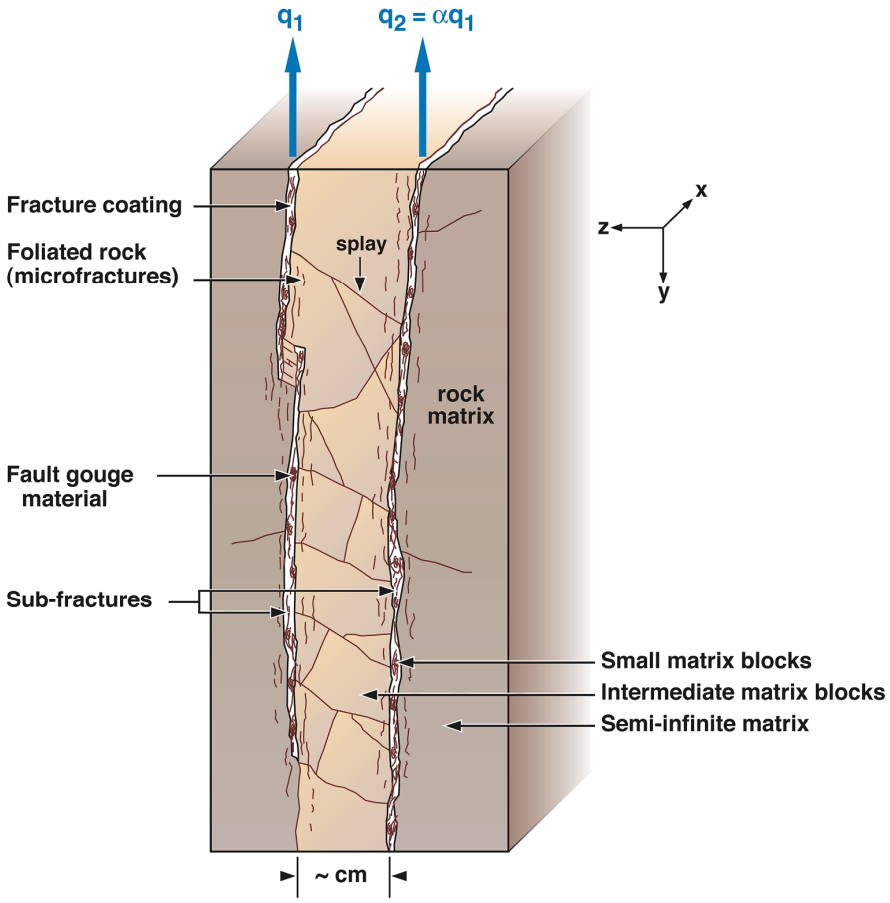

Figure 1. Schematic diagram of the complex fracture model (after Mazurek et al., 2001).

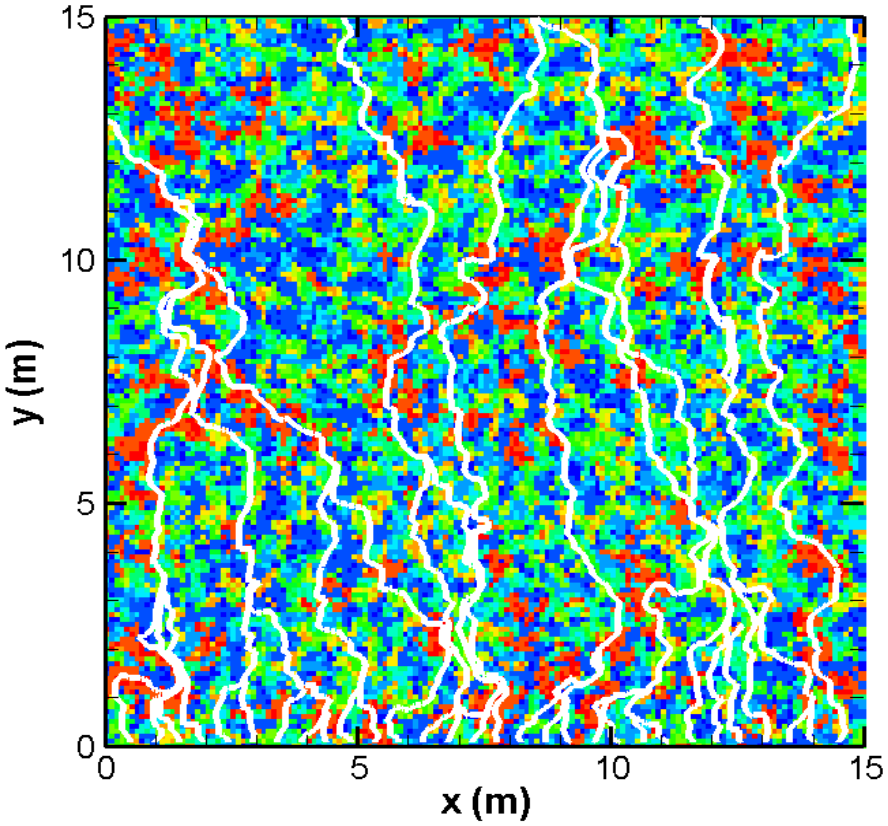

762

763 Figure 2. Fracture transmissivity field T(x,y) for $\sigma_{\log T} = 1.35$: red is high T, blue is low

764 T; flow lines show PA flow field, with flow from bottom to top.

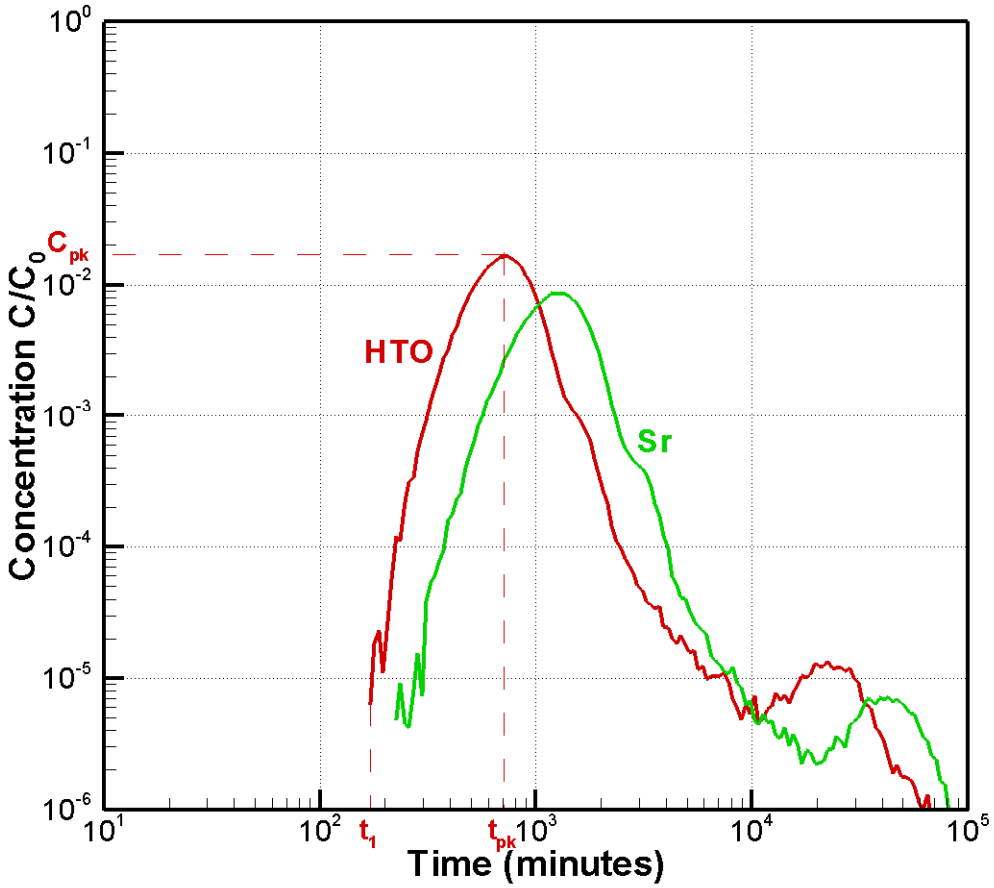

765

766 Figure 3. Site-characterization (SC) tracer breakthrough curves (BTCs) calculated with

767 the complex model, illustrating the three characteristics used to compare BTCs for

768 different models: first arrival time t_1, peak arrival time t_{pk}, and peak height C_{pk}.

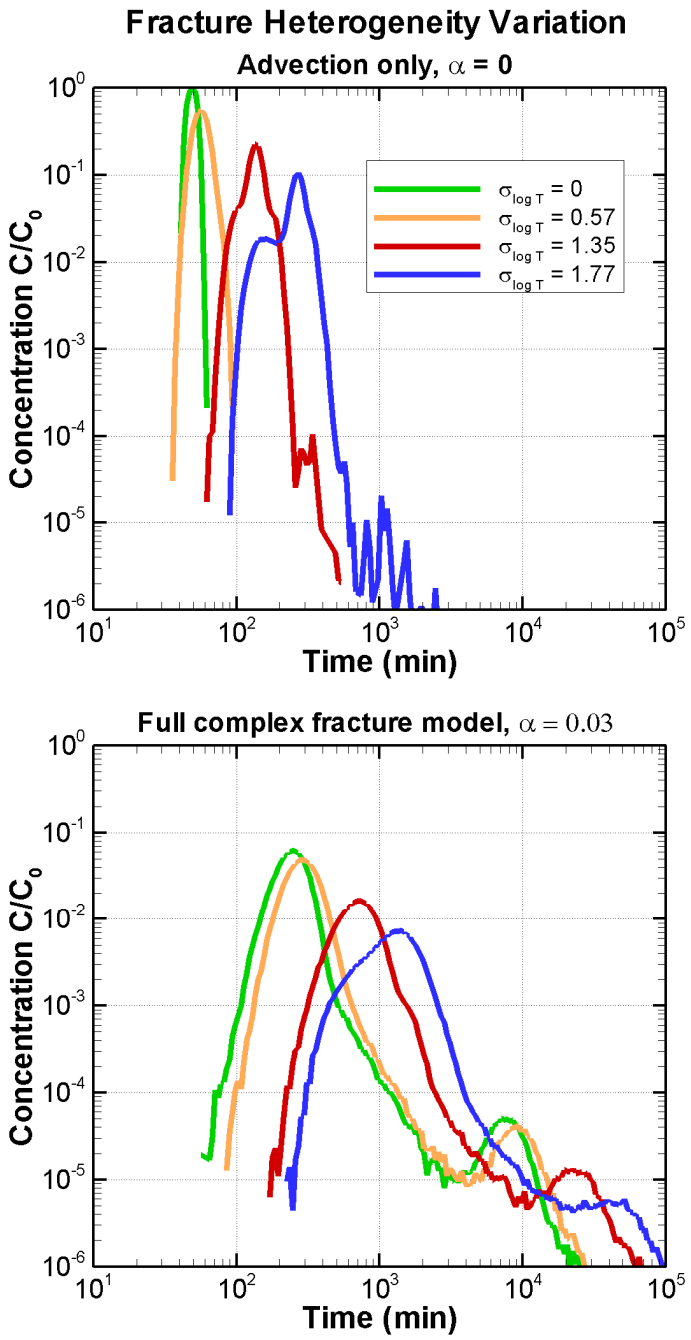

769

770 Figure 4. SC tracer BTCs for cases with different amounts of fracture heterogeneity. Top

771 frame: advection-only (no matrix diffusion or sorption) and only one subfracture ($\alpha = 0$);

772 bottom frame: full complex fracture model with $\alpha = 0.03$, and 25% gouge, 25%

773 intermediate blocks, and 50% semi-infinite matrix.

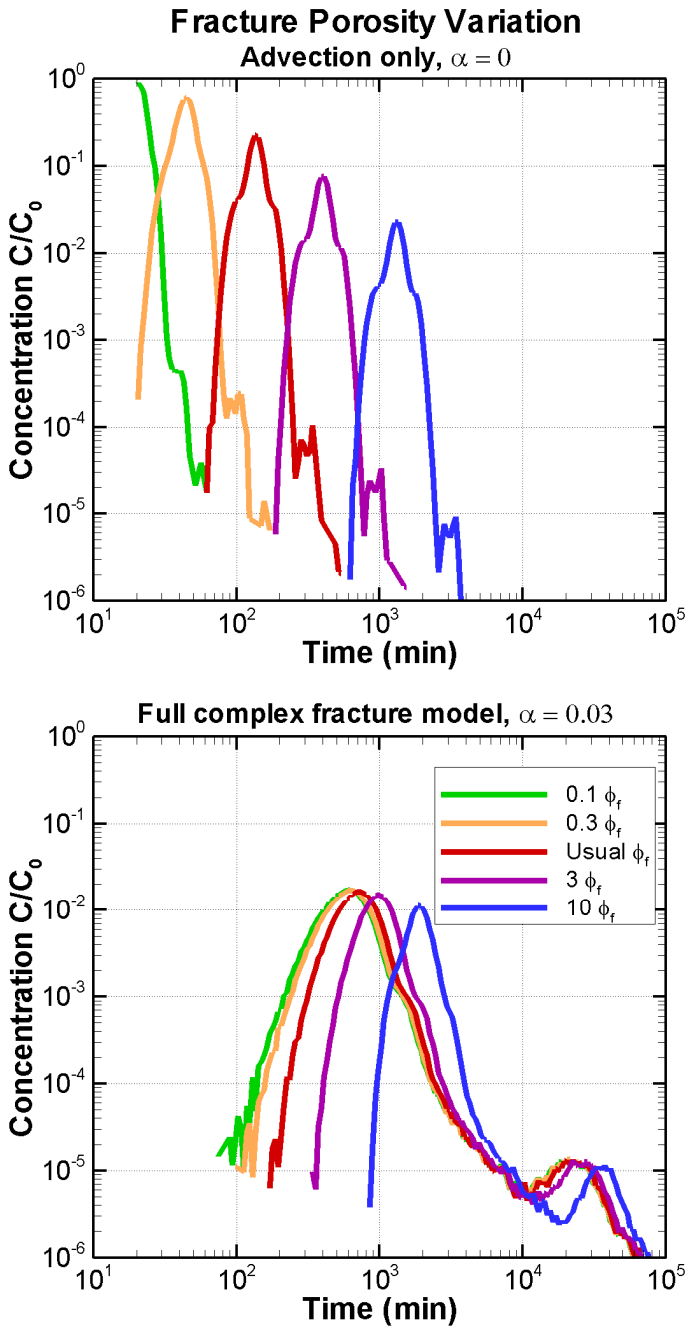

774

775 Figure 5. SC tracer BTCs for cases with different values of mean fracture porosity ϕ_f. Top

776 frame: advection-only (no matrix diffusion or sorption) and only one subfracture ($\alpha = 0$);

777 bottom frame: full complex fracture model with $\alpha = 0.03$, and 25% gouge, 25%

778 intermediate blocks, and 50% semi-infinite matrix.

779

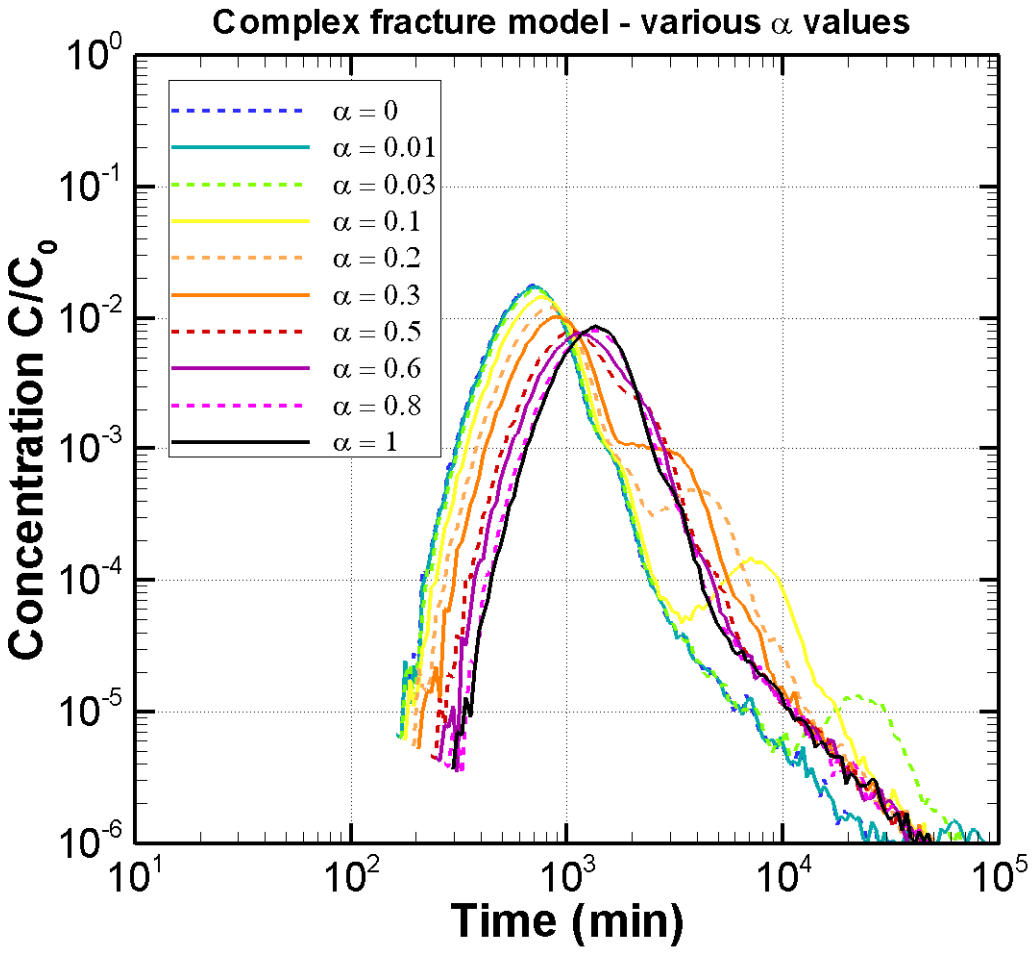

780

781 Figure 6. SC tracer BTCs for various values of fracture structure parameter α.

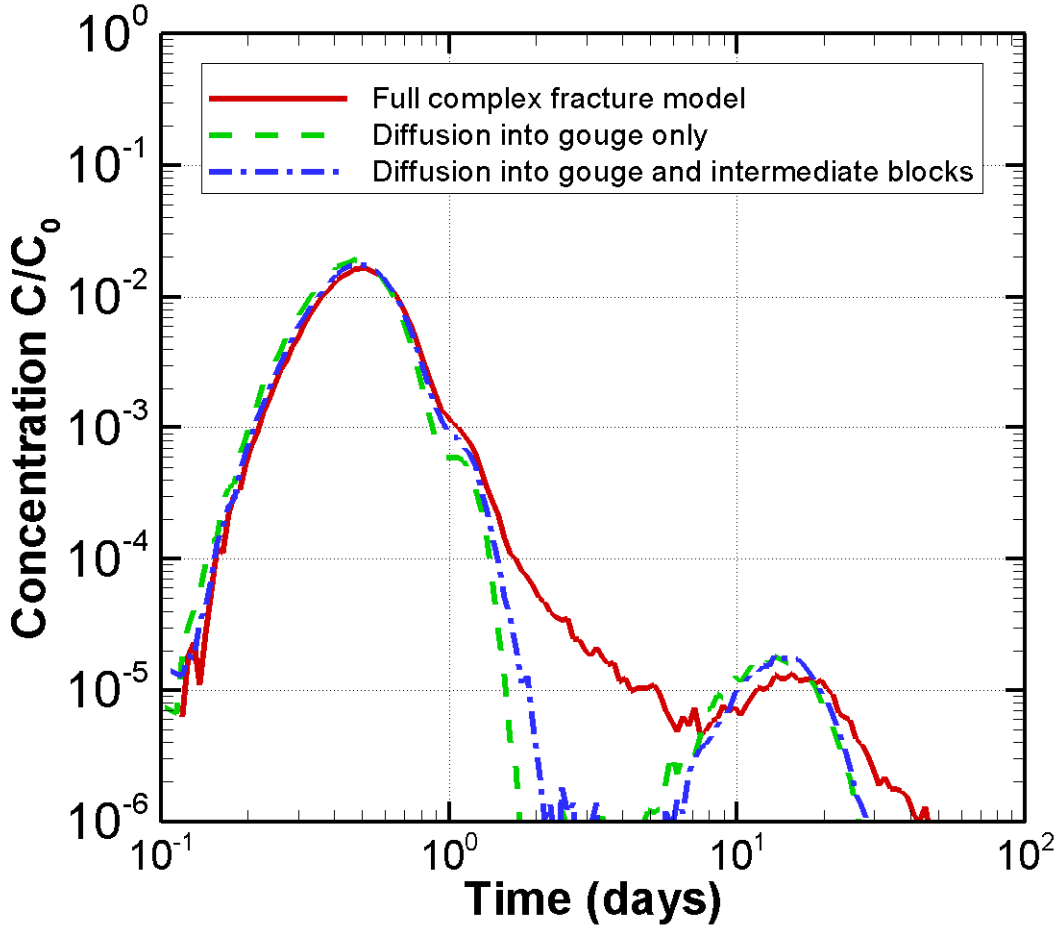

782

783 Figure 7. SC tracer BTCs with diffusion into various materials turned off. Divergence

784 between the different curves illustrates when the effect of diffusion into different rock

785 matrix materials becomes apparent.

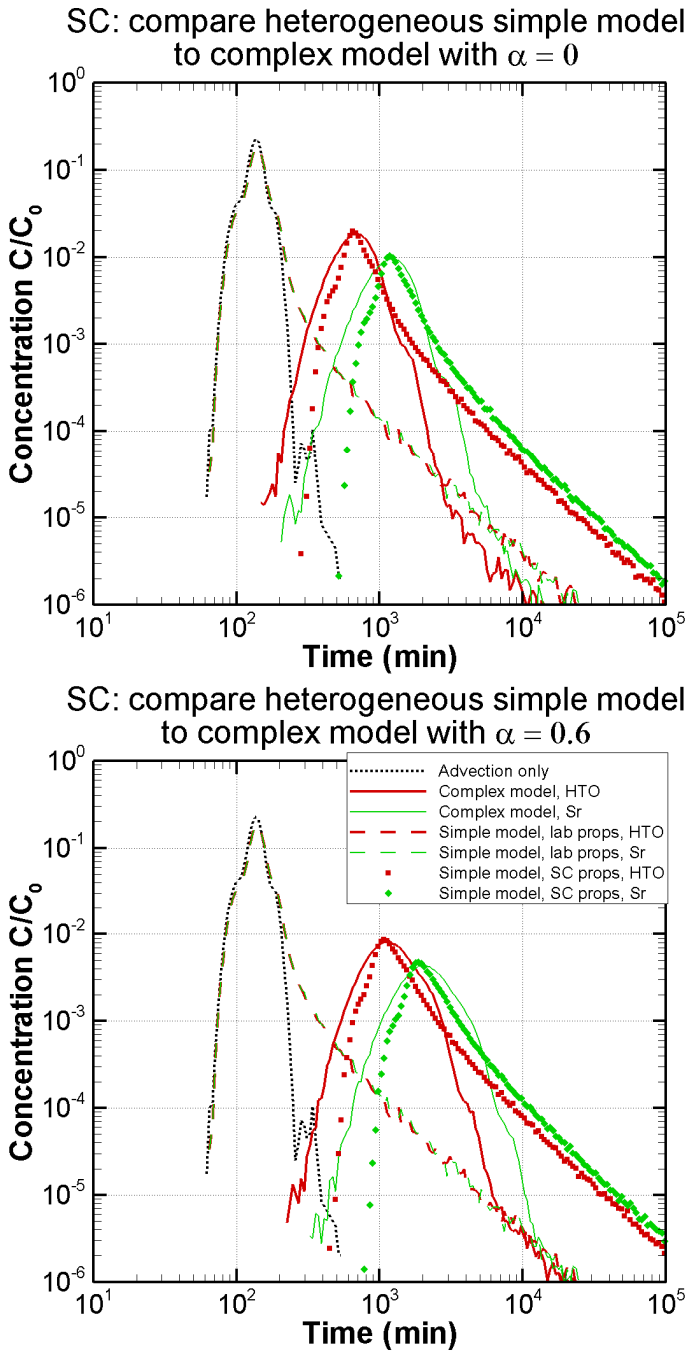

786

787 Figure 8. SC tracer BTCs for the complex fracture model and two versions of the

788 heterogeneous simple fracture model (the original model with laboratory-measured

789 properties and the model calibrated to SC), for two values of fracture structure parameter

790 α. Results for advection-only through a heterogeneous fracture with α = 0 are also

791 shown.

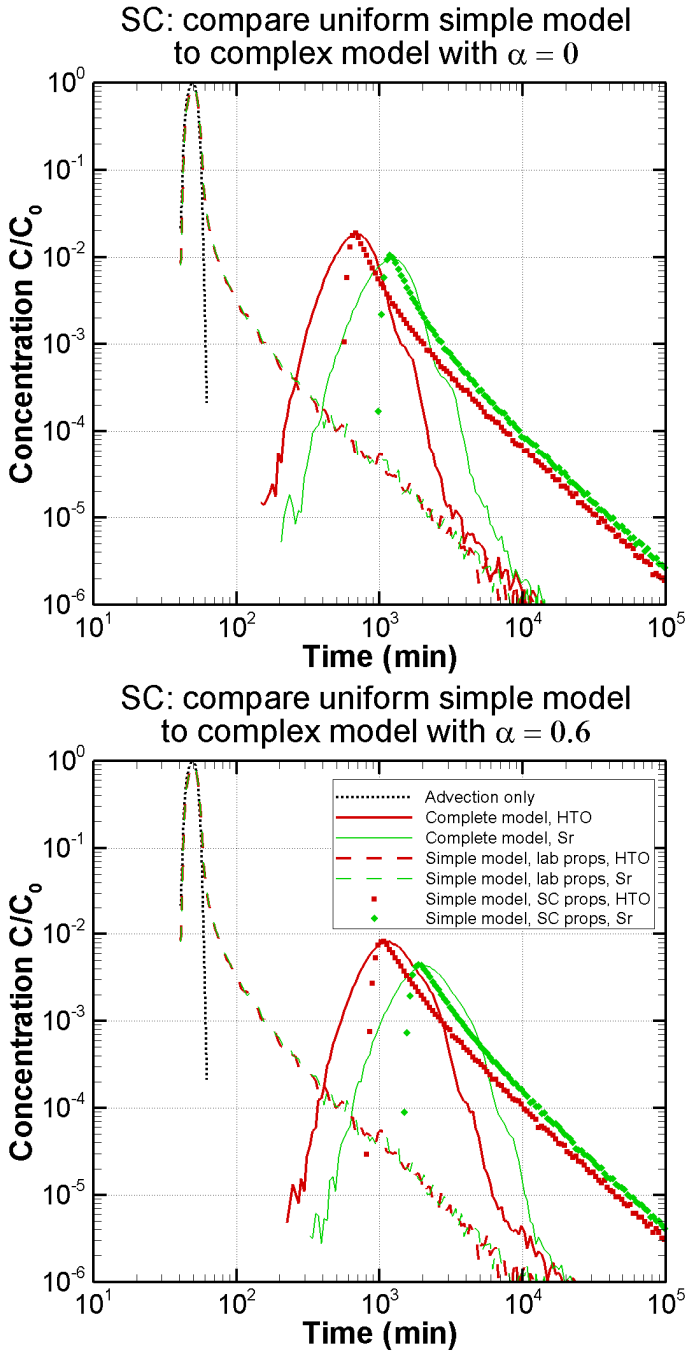

792

793 Figure 9. SC tracer BTCs for the complex fracture model and two versions of the uniform

794 simple fracture model (the original model with laboratory-measured properties and the

795 model calibrated to SC), for two values of fracture structure parameter α. Results for

796 advection-only through a uniform fracture with α = 0 are also shown.

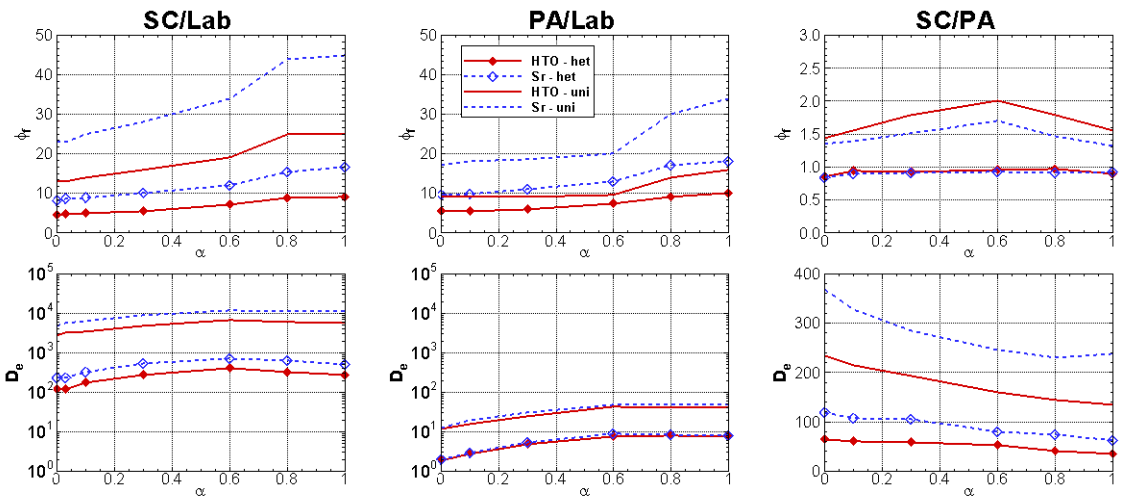

Figure 10. Simplified model parameters required to match SC tracer BTCs for the heterogeneous simple model (het) and the uniform simple model (uni), for a range of α values. The vertical axes show the ratio of the calibrated parameter to the original laboratory-measured values (two left columns) or the ratio of the calibrated parameters for SC and PA (right column).

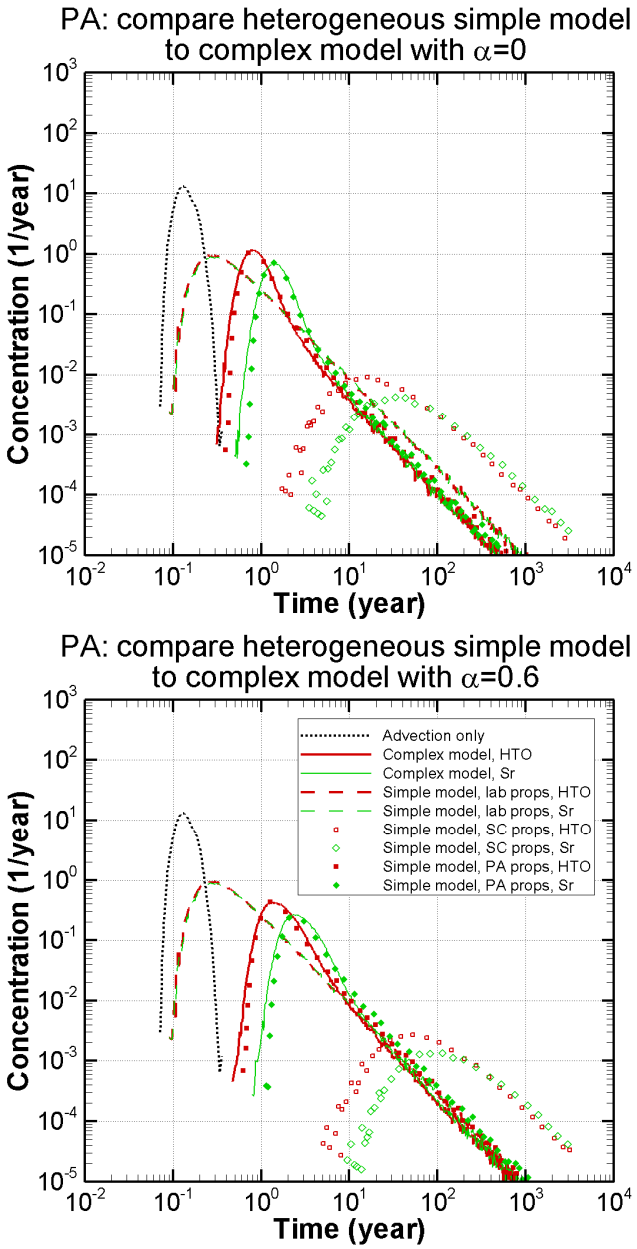

803

804 Figure 11. PA tracer arrivals for the complex fracture model and three versions of the

805 heterogeneous simple fracture model (the original model with laboratory-measured

806 properties, the model calibrated to SC, and the model calibrated to PA), for two values of

807 fracture structure parameter α. Results for advection-only through a heterogeneous

808 fracture with α = 0 are also shown.

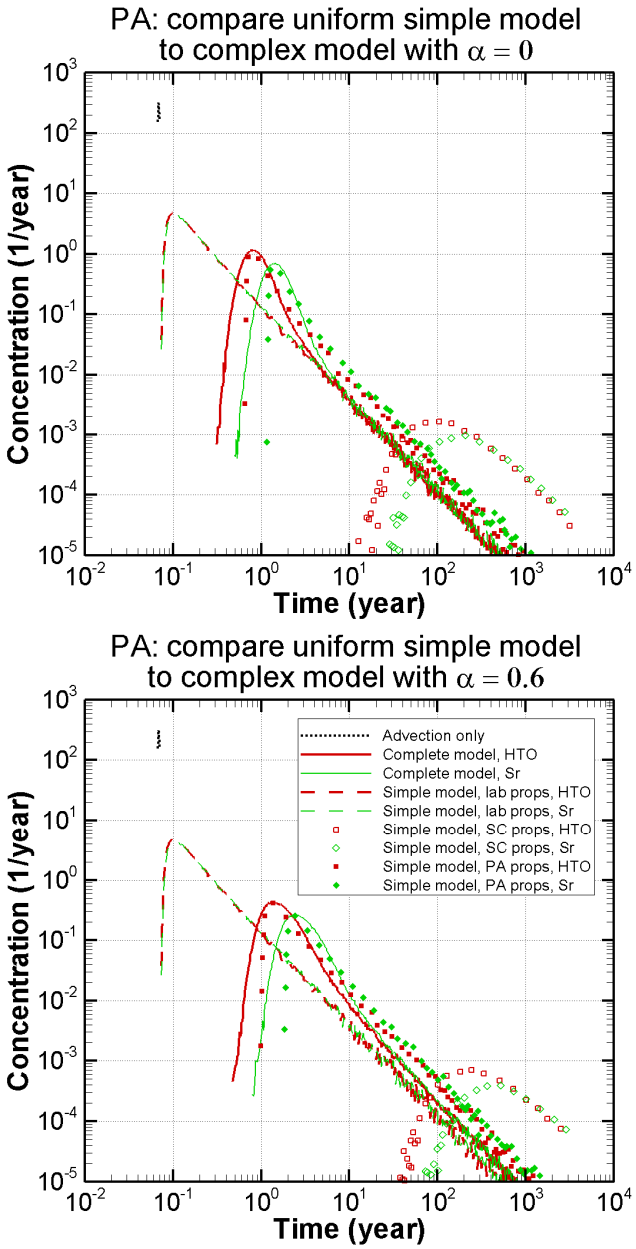

Figure 12. PA tracer arrivals for the complex fracture model and three versions of the uniform simple fracture model (the original model with laboratory-measured properties, the model calibrated to SC, and the model calibrated to PA), for two values of fracture structure parameter α. Results for advection-only through a uniform fracture with α = 0 are also shown.